A High-Performance CW Mobile Channel Sounder

Robert Johnk, Chriss Hammerschmidt, Irena Stange
Institute for Telecommunication Sciences (NTIA/ITS)
U.S. Department of Commerce Boulder Laboratories
Boulder, Colorado 80205, USA
Contact: rjohnk@ntia.doc.gov

***Abstract*— We describe an advanced mobile channel sounder system that has been under development by engineers at NTIA's Institute for Telecommunication Sciences since 2010. We provide a description of the channel sounder and the key system components. We then highlight the flexibility and power of this system by showing a variety of measured and processed radio propagation results obtained using this system. This system has been deployed in numerous outdoor and indoor propagation measurement campaigns. This system has also been used for both in-building and building penetration measurements.**

Keywords—CW, Fast Fading, Doppler; GPS; Geolocation, K-factor, Path Loss, Power Spectrum, Propagation, Rayleigh, Rician, Rubidium, Time Series, Spectrum Analyzer, Vector Signal Analyzer

I. Introduction

A revolution in emerging wireless technologies has placed a major demand on our limited radio spectrum. This has made it paramount for new wireless systems to have high spectral efficiency [1] and to be able to dynamically share spectrum with other wireless systems. More than ever before, there is a need to provide our spectrum policy makers and regulators well-informed and accurate electromagnetic compatibility (EMC) models to insure optimal and trouble-free use of the radio spectrum. A key component of accurate EMC wireless systems modeling and performance predictions is accurate propagation data.

In early 2010, a team of engineers at NTIA's Institute for Telecommunication Sciences (ITS) began the development and design of a new channel sounder system. The team identified four design objectives: 1) develop a fundamental propagation measurement system that is traceable to sampled voltages, 2) develop a simple and spectrally-efficient system that is stable, accurate, and easy to operate, 3) develop a system that acquires a continuous set of data with audio-frequency sampling rates (1–5 kHz) with modest data storage requirements, and 4) achieve accurate measurement of propagation parameters such as path loss, fast-fading, and Doppler power spectrum.

To meet these objectives, ITS engineers have developed a receiver architecture that is based on a Vector Signal Analyzer (VSA) [1],[2]. We provide precise time references on both the receiver and the CW transmitter using rubidium clocks. The VSA receives the transmitted signal for the entire duration of a test and ensures continuity of data acquisition. The in-phase, quadrature (I-Q) data capture format yields high measurement fidelity and flexibility in the extraction of propagation parameters. The use of rubidium clocks ensures high accuracy and stability in the time base of sampled data and permits accurate geolocation of measured data. The ITS system has been deployed in both outdoor and indoor propagation measurement scenarios with excellent results [1]-[3].

II. Channel Sounder Architecture

The ITS channel sounder system is shown in Fig. 1 and a benchtop evaluation setup is shown in Fig. 2. The transmitting side of the system consists of a synthesizer that generates a continuous wave (CW) signal and a power amplifier that boosts the signal to a suitable power level. The amplifier output is fed into a low-pass filter to prevent interference at harmonics of the transmit frequency. The output of the filter is then fed into the transmit antenna and propagates through the radio channel to the receiving system. The received signal is routed to a power splitter, which feeds the VSA and a spectrum analyzer (SA). The VSA is the heart of this measurement system. It takes the received signal and down converts it to a discrete baseband time series of complex in-phase and quadrature samples. The VSA acquires I-Q data at sampling rates in the range of 1–5 kHz. The resulting time series is then transferred to a computer for post processing and data analysis.

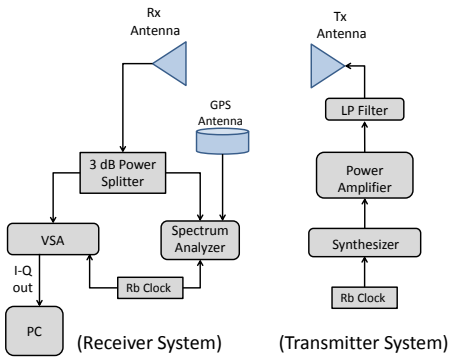

Fig. 1. The ITS CW channel sounder.

This paper was presented at and will appear in the Proceedings of the 2017 IEEE International Symposium on Electromagnetic Compatibility & Signal/Power Integrity (EMCSI), Washington DC, 7-11 Aug. 2017.
EMCSI Proceedings are © IEEE.

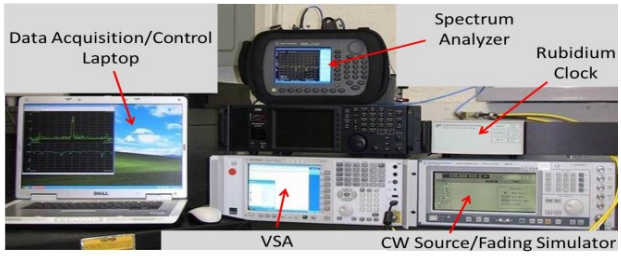

Fig. 2. A benchtop deployment of the ITS channel sounder for system validation and accuracy testing showing the main components.

The other half of the signal is fed to the SA. The SA serves two functions. First, it functions as a signal monitor during mobile drive testing. The VSA that we use for the testing does not have a real-time display during data acquisition, so an active signal monitoring capability is needed to ensure system integrity and functionality. Second, for outdoor mobile measurements, the SA assigns a time stamp and GPS geolocation data to each sweep. This enables us to compare the data from the SA and geolocate selected segments of the VSA data—this is a valuable enhancement for propagation measurements. Geolocated data enables us to develop path loss propagation models as a function of distance. For indoor measurements, the GPS is not active and we need to use a different approach for geolocation of the measured VSA data [3].

Rubidium clocks are used at both the transmitter and receiver to provide high accuracy in measurements and high stability in frequency. The rubidium clock at the receiving end has a fine frequency adjustment to ensure precise alignment of the transmitting and receiving frequencies. Typically, we adjust these frequencies to be within 0.1 Hz for our testing. We have performed an extensive series of outdoor and indoor tests at frequencies ranging from 430 MHz to 5.5 GHz for power levels from 20 mW to 70 W [1]-[3].

III. Signal Processing

The signal processing for the channel sounder is shown Fig. 3. In order to estimate the basic path loss, we start with the VSA I-Q data. We first compute the magnitude of the I-Q time series and then apply a windowed average over the resulting time-series to compute a local mean. Fig. 4 shows an example of a fast-fading time series and a local mean that we generated using the benchtop setup of Fig. 2. The time series was generated with the CW source set at 3.5 GHz, and the simulator configured for Rayleigh fading at a speed of 20 mph (8.94 m/s). The envelope exhibits rapid and large variations which is characteristic of Rayleigh fading [4],[5]. To reduce the effects of the fast fading, we apply a centered-sliding window of fixed width to the fast-fading envelope and perform a straight linear average of the voltage data within the window. Once an average is computed, the window is advanced to the right by one data sample and another average is computed. This process is repeated until the window reaches the end of the time series. The red line in Fig. 4 shows the average voltage obtained from a 0.5 s wide window. The average voltage is far smoother and has less variation. This averaged

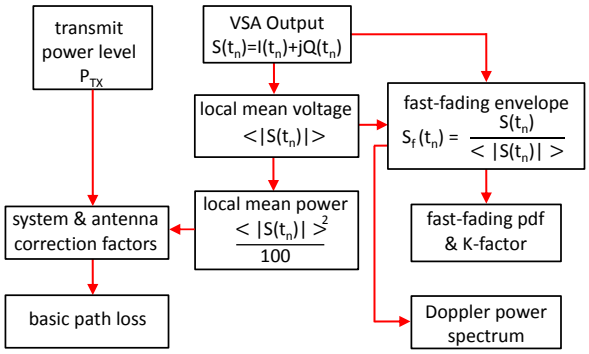

Fig. 3. Signal processing to obtain basic path loss and fast fading parameters, and Doppler power spectrum.

voltage is the so-called local mean [4]. We typically use an averaging window with a temporal width of 0.5 to 2 s. In Fig. 4, the 0.5 s wide averaging window width has an equivalent spatial extent of 52 wavelengths at 3.5 GHz and a speed of 20 mph (8.94 m/s). The VSA is a voltage measurement device, so we can now compute the power of the local mean by squaring the I-Q envelope and dividing by 100 (this assumes a 50 Ω system).

We use the local mean voltage in combination with the measured power at the input of the transmit antenna, system cable losses, and the gains of the transmit and receive antennas to compute the basic path loss:

$$BPL\ (dB) = P_t - P_{lm} + (G_t - L_t) + (G_r - L_r)\,, \qquad (1)$$

where P_t and P_{lm} are the transmitting and local mean received power levels in dBm. G_t and G_r are the gains of the transmit and receive antennas in dBi. The system loss between the transmit antenna and the transmitter output port is L_t. The corresponding loss on the receive side is L_r. Basic path loss as defined in (1) is the difference between the transmitted and received power levels with corrections for antenna gains and system losses.

The right side of Fig. 3 shows the process by which the propagation parameters are computed from the normalized

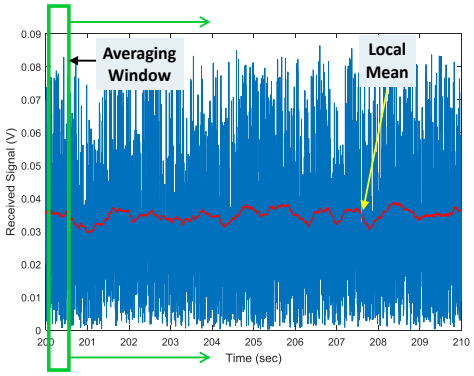

Fig. 4. Computing a local mean (red trace) with a sliding window on the fast-fading envelope (blue trace).

fast-fading envelope. The VSA I-Q output is divided by the corresponding local mean to yield a normalized fast-fading time series $S_f(t_n)$. We detrend the received I-Q data by removing the slower variations due to shadowing and path loss effects. The result is an I-Q time series that contains the fast-fading variations due to motion through the mobile channel. We show an example of a detrended time series in section V.

We use $S_f(t_n)$ to perform additional processing. We can select a time segment of $|S_f(t_n)|$ and compute an estimate of the probability density function (PDF) of the fast-fading envelope. The length of this segment is a function of the speed, operating frequency, and propagation environment. If the estimated PDF is Rician, we can readily compute K-factors, which is the ratio of the signal power in the line-of-sight (LOS) signal to the signal power from local scatterers around the mobile receiving antenna. In section V, we show estimated PDFs and associated K-factors obtained for actual mobile channel measurements.

The Doppler power spectrum is obtained directly from the normalized time series, $S_f(t_n)$. To do this, we select a time interval of $S_f(t_n)$ and apply Welch's method [6] to compute the Doppler power spectrum. The first step in Welch's method is to divide the selected interval into consecutive segments. The results that we present in section VI are for consecutive segments that are non-overlapping. We apply a discrete Fourier transform to the complex I-Q time series elements and square the magnitude of the result to obtain a power spectrum for a given segment. The final result is obtained by averaging the power spectra over all the segments. This averaging reduces the variance in the estimated power spectra. We show some examples of this in section VI.

IV. Mobile Channel Measurements

A team of ITS engineers recently carried out a mobile channel measurement campaign at 3,500 MHz in Boulder, Colorado. The transmitting system was deployed on top of Kohler Mesa, located on the campus of the U.S. Department of Commerce Laboratories. Fig. 5(a) shows the transmitting antennas, and Fig. 5(b) shows the view looking east towards the residential neighborhoods of Boulder. The transmitting antenna has an omnidirectional pattern in the azimuthal plane and a gain of 9 dB. The transmitted power level was set at 47 W and maintained at a constant level for the tests. The drive test van is shown in Fig. 5(c). The van has a custom-designed aluminum ground plane on the roof to facilitate antenna installation and pattern control. A 2 dB gain conical receiving antenna was placed on a short mast on top of the ground plane. The receiving antenna also has an omnidirectional pattern in the azimuthal plane. The VSA, SA, and rubidium clock were placed in special racks that are cushioned against shock and vibrations. The equipment is powered by an on-board 5 kW generator that provides 120 V AC.

A drive test was performed in south Boulder. The drive test route is shown in Fig. 6. The route began near the top of the map and progressed in a serpentine fashion through the Martin Acres subdivision. The route then progressed through the Claremont-Drexel neighborhood. The drive continued to the top of the NCAR Mesa and then back to the ITS facility. We maintained a nominal speed of 20 mph for most of the drive. It took just over one hour to complete the drive.

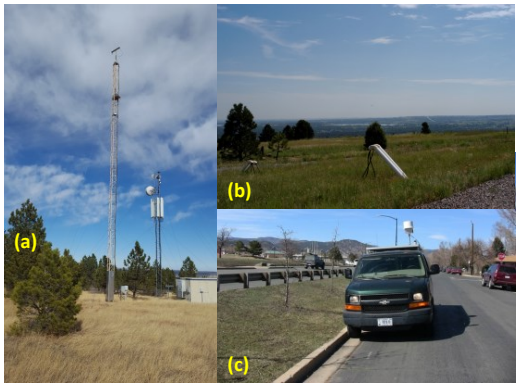

Fig. 5. (a) The transmitting antenna and equipment shelter on Kohler Mesa. (b) The view looking east from the transmitting antenna towards Boulder, CO. (c) The ITS-designed van that carries the receiver.

The VSA was configured for a total bandwidth of 3 kHz and a sampling rate of $f_s = 3{,}840$ Hz. This rate was selected to ensure adequate sampling of received signals with Doppler shifts of up to 300 Hz. The SA was configured in the zero-span mode [7] with sample detection with a bandwidth of 3 kHz to capture the I-Q envelope of the received signal. The SA sweep rate was set at 0.5 s. A total of 461 samples were captured in each sweep. Both VSA and SA data were acquired for the entire duration of the drive.

V. Raw and Detrended Signals

We now show some results from the western section of Martin Acres shown in Fig. 7. The first portion of the drive (part A) occurs inside a residential area and non-line-of-sight conditions (NLOS) are experienced. As we transition into part B, line-of-sight (LOS) conditions occur. We then re-enter the residential area in Part C and NLOS conditions occur again. Fig 8(a) shows the VSA received I-Q envelope, along with the local mean obtained from a 0.5 s moving-average window. In parts A and C, the I-Q envelope experiences rapid variations in excess of 50 dB. Over the middle portion of part B, we observe significantly reduced signal variations due to the LOS signal from the transmitter. When we detrend the I-Q data using the local mean and compute the magnitude of the complex time

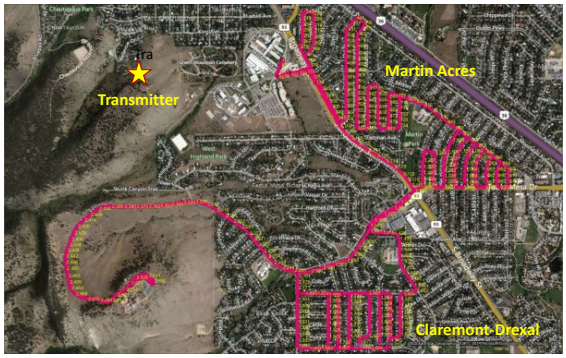

Fig. 6. Boulder drive route. The yellow star denotes the transmitter. Martin Acres and Claremont-Drexel are residential neigborhoods.

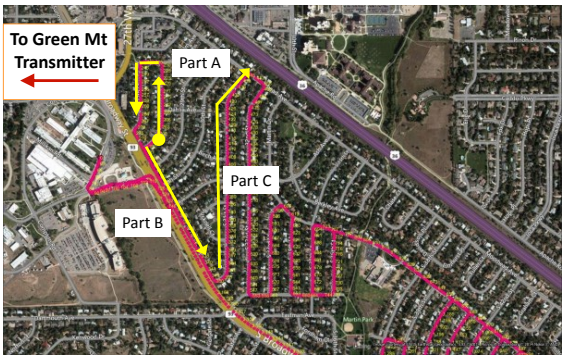

Fig. 7. A section of the drive test showing three representative parts of the drive test. This map has approximate dimensions 1.2 km x 2 km.

series, we obtain the result of Fig. 8(b). The result is the fast-fading envelope in which the slow variations due to path loss and shadowing have been suppressed. The average level of the detrended signal is nearly constant. The levels of signal variations are larger for NLOS, and smaller for LOS conditions.

We can also use the envelope of Fig. 8(b) to compute fast-fading distributions. We first convert the envelope from dBV to linear voltage and then apply a Matlab® maximum likelihood estimation (MLE) routine to estimate a probability density function (PDF) and its associated parameters. Fig. 9(a) shows a PDF obtained from a 14 s interval in part A of the drive. The Rayleigh and Rician fits are nearly identical, which is indicative of NLOS conditions. The estimated K-factor is 0.4 which indicates a small LOS component. When we process a similar time interval in part B, the Rician distribution of Fig. 9(b) is obtained. The result is a centralized and symmetric distribution, which is attributed to a strong LOS component.

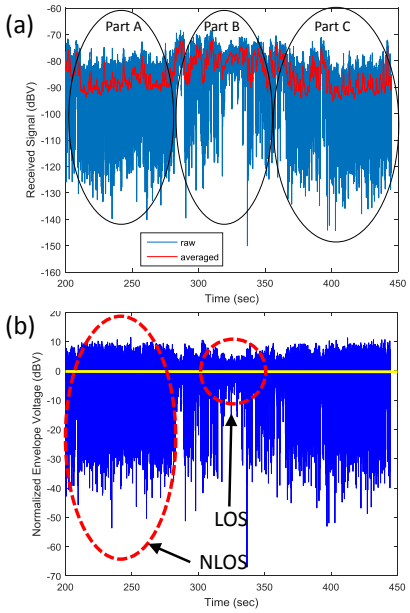

Fig. 8. (a) Raw VSA signal with the drive sections A, B, and C. (b) Detrended signal showing both NLOS and LOS behaviors.

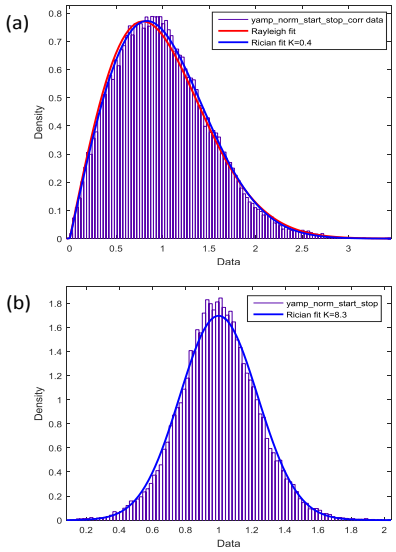

Fig. 9 (a) Section C fast-fading envelope with Rayleigh and Rician MLE fits. (b) Section B fast-fading envelope with Rician MLE fit.

The K-factor in this case is 8.3.

VI. Doppler Power Spectrum

We computed the Doppler power spectrum over several sections of the drive test shown in Fig 10. For each case, we used Welch's method to process a 5 s record of $S_f(t_n)$. We divided the segment into five non-overlapping intervals. The three sections that we analyze have distinctly different propagation conditions. In section A, the van is driving away from the transmitting antenna at 30 mph. This section experiences strong LOS condition. Section B has both a dominant LOS condition and reflections from a hill that is adjacent to the road. Section C is in a residential neighborhood, and NLOS conditions occur there. The resulting baseband power spectra are shown in Fig. 11. The section A results are shown in Fig. 11(a). In this case, we have a dominant LOS spectral line at -156 Hz. The downward Doppler shift is due to the movement of the van away from the transmitter. In Fig. 11(b), we see the transmitter spectral line with additional lines due to scattering from a hill that is adjacent to the road. Here, all the power spectral lines have negative Doppler, which

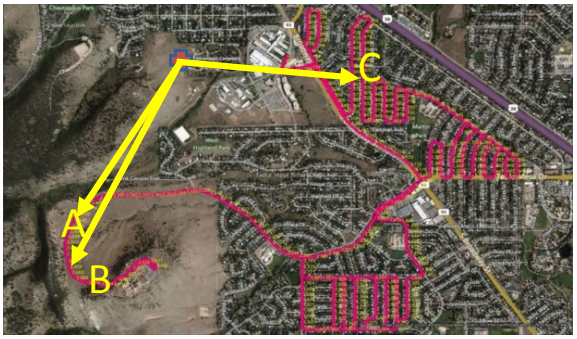

Fig. 10. Three sections in which the baseband Doppler power spectrum is computed on the Boulder drive test.

This paper was presented at and will appear in the Proceedings of the 2017 IEEE International Symposium on Electromagnetic Compatibility & Signal/Power Integrity (EMCSI), Washington DC, 7-11 Aug. 2017.

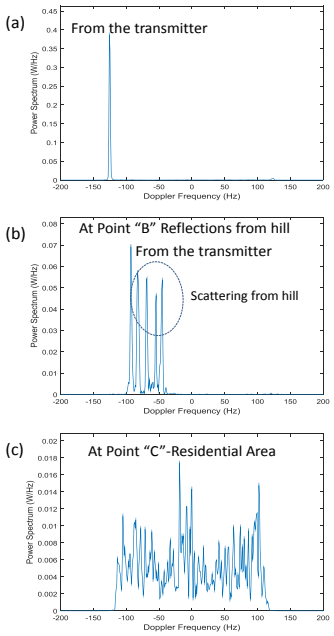

Fig. 11. (a) Location A Doppler power spectrum with a dominant transmitter-receiver LOS path. (b) Location B Doppler power spectrum with scattering from the hill. (c) Location C power spectrum

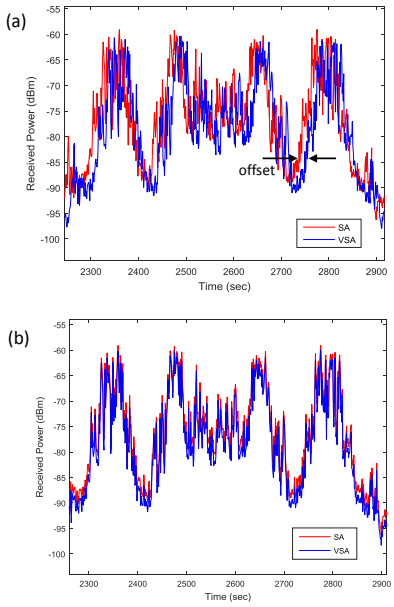

Fig. 12. Spectrum analyzer trace-averaged power and VSA window-averaged rceived power. (a) Unaligned data. (b) After VSA timebase correction.

indicates that the van is moving away from both the transmitter and the hill. The power spectrum of Fig. 11(c) has a much different character. The van is immersed in a residential neighborhood in a rich scattering environment. The resulting power spectrum is diffuse with a distribution of scattering components in the range of -115 Hz to 115 Hz. This indicates that there is a distribution of scatterers surrounding the van. The fact that there is not a dominant spectral line is characteristic of an NLOS condition.

VII. Geolocation of VSA Data

Our channel sounder uses an SA in tandem with the VSA. The spectrum analyzer is configured to capture data in the zero-span mode with sampling detection and a resolution bandwidth of 3 kHz [7]. For the Boulder measurements, we set the sweep rate of the spectrum analyzer at 0.5 s and capture the trace of the I-Q envelope of the received signal during the sweep. Due to a combination of instrument architecture and the time it takes to reset for a new sweep, the SA captures a new trace at a rate of once per second. The SA uses the GPS receiver information to assign a GPS time and location stamp to each trace. We then compute the average power of each sweep. The result of this process is a series of time-stamped and geolocated SA power measurements. We use this geolocated time series to discipline the window-averaged VSA data.

Fig. 12(a) shows a plot of the window-averaged VSA data and the averaged SA data. The signals are very similar except there is a time offset between them. This offset is due to combination of the times in which we initiate data acquisition with the VSA and the SA and data transfer latencies. We typically see offsets in the range of 2-15 seconds. In Fig. 12(b) we have shifted the VSA series to align it with the SA data. The resulting time series closely agree. In order to illustrate the effects of time alignment, we plot the power computed from the VSA window-averaged voltage versus the SA power for a sequence of different time offsets t_d. We show some results in Figs. 13(a)-(c). In Fig. 13(a), the offset between the VSA and the SA is 13 s. In this case, the VSA and SA data are not well correlated which manifests itself in the cloud-like appearance of the data. The data are time-aligned in Fig. 13(b) with t_d = 12 s and the results are both highly-correlated and tightly clustered. In Fig. 13(c), we have decreased the offset to 11 s and, once again, the data are not well correlated.

We time-align the data by repeatedly shifting the VSA data and performing a linear regression fit to the SA data at each step. For each regression, we compute the sum of residuals of the data to the estimated fit. Time-alignment occurs when the sum of residuals is minimized. This occurs when the SA and VSA data are highly correlated. We have developed a simple one-variable optimization routine that automates this process and quickly aligns the SA and VSA data. Once the optimization is complete, we assign the SA geolocation stamps to the corresponding VSA data points. One drawback of this approach is that we cannot geolocate all of the VSA samples. We can only geolocate a given VSA sample that aligns with a corresponding SA sample.

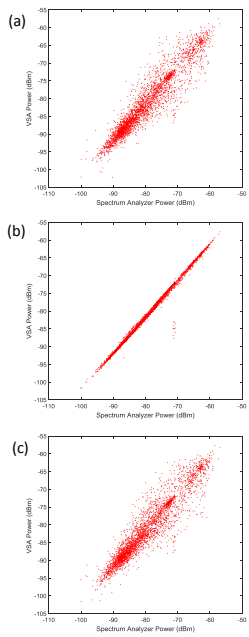

Fig. 13. VSA window-averaged data vs. SA date for different time delays. (a) t_d = 13 s. (b) t_d= 12 s. (c) t_d=11 s.

Fig. 14 shows basic path loss vs. distance for the drive test that we obtained using this time-alignment procedure. Here we use the geolocated VSA data to construct this plot. In addition to the measured basic path loss, we have plotted the free-space path loss results [8]. The complexity of the drive test propagation environment is highlighted by the large spread of data. This is the result of the combined effects of terrain and the clutter effects of buildings, houses, and vegetation. We also see data that exhibits path losses that are lower than free space. This occurs in the strong LOS portions of the drive where nearby scatterers combine constructively to yield signal levels in excess of the direct path component.

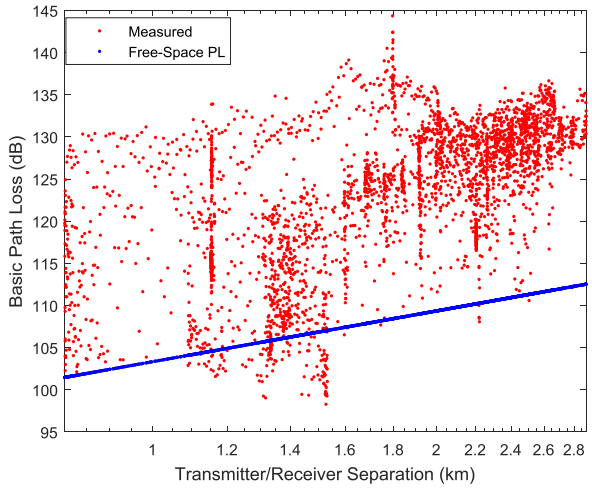

Fig. 14. Basic path loss vs distance (red) for the Boulder drive test. The blue curve is the correspnding free-space path loss.

VIII. Conclusions

We have described an ITS-developed CW channel sounder that has excellent performance characteristics. This system can measure a number of propagation parameters such as path loss, fast-fading characteristics, Rician K-factors, and baseband Doppler power spectrum. This system has been deployed in a number of measurement campaigns since 2011. We are currently improving this system by enhancing its geolocation capabilities and dynamic range. This system will continue to produce reliable data to inform national spectrum policy for many years to come.

Acknowledgment

The authors would like to thank Keith Gremban, Andy Thiessen, Eric Nelson, and Mike Cotton of the Institute for Telecommunication Sciences for their support of this research.

References

[1] Robert Johnk, Chriss Hammerschmidt, Mark McFarland, John Lemmon, "A fast-fading measurement system," IEEE Int. Symp. EMC, August 6-10, 2012 pp. 584-589.

[2] Chriss Hammerschmidt and Robert Johnk, "Extracting clutter metrics in the 1755-1780 MHz band, Proc. of the IEEE Military Communications Conf., Baltimore, MD, Nov. 1-3, 2016.

[3] Nadia P. Yoza, Narrowband 5 GHz Mobile Channel Characterization, M.S. Thesis, Interdisciplinary Telecommunications Program, University of Colorado at Boulder, 2015.

[4] J. D. Parsons, The Mobile Radio Propagation Channel, John Wiley & Sons, New York, New York, 2000.

[5] Fernando Perez Fontan and Perfecto Marino Espineira, Modelling the Wireless Propagation Channel: A Simulation Apporach with Matlab, John Wiley & Sons, New York, New York, 2008.

[6] P.D. Welch, "The use of the fast fourier Transform for the estimation of power spectra: A method of time-averaging over short, modified periodograms", IEEE Trans. on Audio and Electroacoustics, AU-15(2), pp. 70-73, 1967.

[7] Chistoph Rauscher, Fundamentals of Spectrum Analysis, 5th Edition, Rohde & Schwartz, Colombia, MD, 2011.

[8] Simon Saunders and Alejandro Aragon-Zavala, Antennas and Propagation for Wireless Communication Systems, John Wiley & Sons, New York, New York, 2007.

This paper was presented at and will appear in the Proceedings of the 2017 IEEE International Symposium on Electromagnetic Compatibility & Signal/Power Integrity (EMCSI), Washington DC, 7-11 Aug. 2017.